Surface Chemistry

International Edition: DOI: 10.1002/anie.201501830
German Edition: DOI: 10.1002/ange.201501830

The Magic Au_{60} Nanocluster: A New Cluster-Assembled Material with Five Au_{13} Building Blocks**

*Yongbo Song, Fangyu Fu, Jun Zhang, Jinsong Chai, Xi Kang, Peng Li, Shengli Li, Hongping Zhou, and Manzhou Zhu**

Abstract: *Herein, we report the synthesis and atomic structure of the cluster-assembled $[Au_{60}Se_2(Ph_3P)_{10}(SeR)_{15}]^+$ material. Five icosahedral Au_{13} building blocks from a closed gold ring with Au–Se–Au linkages. Interestingly, two Se atoms (without the phenyl tail) locate in the center of the cluster, stabilized by the Se-$(Au)_5$ interactions. The ring-like nanocluster is unprecedented in previous experimental and theoretical studies of gold nanocluster structures. In addition, our optical and electrochemical studies show that the electronic properties of the icosahedral Au_{13} units still remain unchanged in the penta-twinned Au_{60} nanocluster, and this new material might be a promising in optical limiting material. This work offers a basis for deep understanding on controlling the cluster-assembled materials for tailoring their functionalities.*

Metal nanoclusters (NCs) with atomic precision have attracted wide interest in recent research.[1] Among the metal NCs, the gold NCs protected by phosphine,[2–12] thiolate,[13–22] selenolate,[23–27] or co-protected by thiolate and phosphine[28–30] are particularly promising owing to their novel properties and wide applications in various fields such as biomedicine,[31] chemical sensing,[32] bioassays,[33] bio-labeling,[34] magnetism,[35,36] and catalysis.[37,38] Nevertheless, if you want to make full use of the gold NCs, the assembly of structural building blocks into functional materials remains a challenge, which are also called cluster-assembled materials.

Teo et al. reported the $(p\text{-Tol}_3P)_{12}Au_{18}Ag_{20}Cl_{14}$ cluster with three 13-atom cluster units sharing three Au vertices, and this cluster was named a cluster of clusters.[39] Thereafter, the research groups of Tsukuda[28] and Jin[29] reported the structure and the optical properties of the rod-like 25-atom cluster, which is constructed by bridging two icosahedral Au_{13} clusters with thiolates sharing a vertex atom. Furthermore, theoretical studies for the cluster-assembled materials also been reported by Nobusada and Iwasa,[40] and it is proposed that the electronic properties of the "building block" (Au_{13}) would remain almost unchanged in the cluster-assembled materials (such as $[Au_{25}(PPh_3)_{10}(SR)_5Cl_2]^{2+}$ or theoretical $[Au_{37}(PPh_3)_{10}(SR)_{10}Cl_2]^+$). All in all, the icosahedral Au_{13} cluster acts as a fundamental building block, and plays an important role in realizing the cluster-assembled materials. Nonetheless, little is known about the cluster-assembled materials, and several fundamental questions await to be answered: 1) Is it possible to obtain a larger cluster-assembled material (with more than three "building blocks") in experiment? 2) How are the Au_{13} units arranged in the cluster-assembled materials, linear or other modes? 3) Would the electronic properties of the "block building" remain unchanged in the larger cluster-assembled materials? The answer to these questions is of crucial importance for a deep understanding of the cluster-assembled materials, and the experimental evidences are highly necessary.

Herein, we successfully synthesized gold NCs co-capped by selenolate and phosphine. And its crystal structure was determined by X-ray crystallography (Figure 1 A), and the accurate composition was defined as $[Au_{60}Se_2(Ph_3P)_{10}(SePh)_{15}](SbF_6)$ (Au_{60} for short; see Figure S1 in the Supporting Information). It was found that Au_{60} contains five icosahedral Au_{13} building blocks, and each adjacent two Au_{13} units share a vertex gold atom in a cyclic fashion (i.e. five

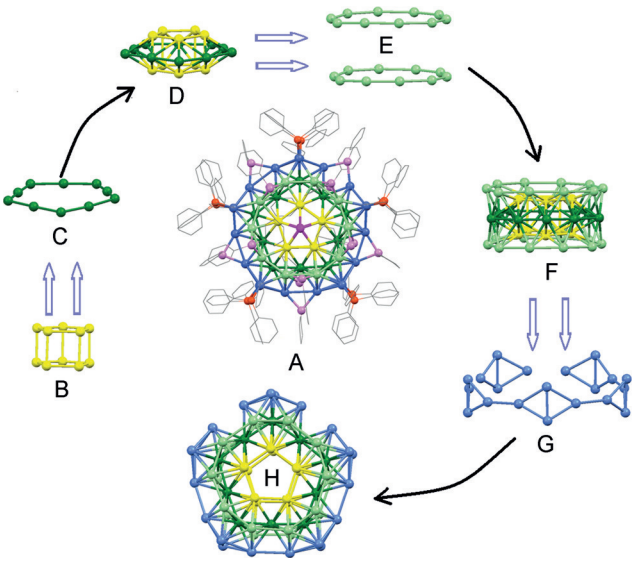

Figure 1. Total structure of the $[Au_{60}Se_2(PPh_3)_{10}(SePh)_{15}]^+$ cluster. (color labels: yellow/green/light green/light blue = Au; violet/magenta = Se; orange = P; gray = C, for clarity all H atoms are not shown).[43]

[*] Y. Song, F. Fu, Dr. J. Zhang, J. Chai, X. Kang, Prof. P. Li, Prof. S. Li, Prof. H. Zhou, Prof. M. Zhu
Department of Chemistry and
Centre for Atomic Engineering of Advanced Materials
Anhui University, Hefei, Anhui, 230601 (P. R. China)
E-mail: zmz@ahu.edu.cn

[**] We acknowledge financial support by NSFC (grant numbers 21072001, 21201005, and 21372006), the Ministry of Education and Ministry of Human Resources and Social Security, the Education Department of Anhui Province, Anhui Province International Scientific and Technological Cooperation Project, 211 Project of Anhui University.

Supporting information for this article is available on the WWW under http://dx.doi.org/10.1002/anie.201501830.

vertex gold atoms in total $5\times13-5=60$), which also abides the rule of cluster-assembled clusters.

To clarify the details of the atom-packing structure, we exhibited the ring-like Au_{60} core in Figure 1H, and compared its structure with the double icosahedral Au_{13} cluster constructed Au_{25} nanocluster. In the Au_{25} nanocluster, the two icosahedral Au_{13} clusters are bridged with thiolates, sharing a vertex gold atom and terminated by two chlorine atoms. By contrast, the Au_{60} nanocluster is terminated by sharing a vertex gold atom without the chlorine atoms and forms a closed gold ring. The outside diameter of the ring is about 14.00 Å and the inside diameter is about 4.20 Å (the calculation method is displayed in Figure S2), resulting in an overall cluster dimension of about 1.7 nm, where the diameter of gold atom is taken to be 1.5 Å.

Due to the ring-like structure, Au_{60} can be divided into four layers from inside to outside (I, II, III, IV as shown in Figure 1B, 1C, 1E, and 1G, respectively, 60 (Au) = 10 + 10 + 20 + 20). For a more detailed anatomy of the total structure, we start with the innermost layer (Figure 1B), which looks like a pentagonal prism: both the top and the bottom are pentagons (the angle sum of pentagon: 539.95°), and the range of the Au–Au bond length is from 2.741 to 2.759 Å. In addition, the four Au atoms in each side face are almost in the same plane (the angle sum of quadrangle: 359.92°). Interestingly, layer II (Figure 1C) is a closed decagon constituted by 10 Au(0) atoms—the Au atoms are all connected to the neighboring Au atoms, and this observation has been noted in other gold NCs. The average Au–Au bond length is 2.803 Å. Layers I and II together give rise to an incomplete bipyramid, which looks like an UFO (Figure 1D). Layer III contains two circular rings, and each of them consists of 10 Au atoms (Figure 1E), and the average Au–Au bond length is 3.011 Å. As shown in Figure 1F, the two circular rings are just like a cylindrical barrel, and hold the "UFO" inside it. Finally, the remaining 20 Au atoms can be seen as five rhombuses connected by the Au−Au bonds, which looks like a crown (Figure 1G). In each rhombus, the average Au-Au bond length is 2.974 Å.

Alternatively, Au_{60} can also be viewed as a cluster-assembled material, and can be divided into five icosahedral Au_{13} building blocks clipped together by five Au–Se–Au linkages (Figure 2). In each Au_{13} unit, the Au–Au distances are in the range of 2.60–3.12 Å. The bond distances are similar to those in the $[Au_{13}(PMe_2Ph)_{10}Cl_2]^{3+}$ and $[Au_{25}(PPh_3)_{10}(SR)_5X_2]^{2+}$ NCs.[4,28,29] However, compared with the rod-like Au_{25}, the Au–Au bond distances between two adjacent Au_{13} units are significantly different and can be generally classified into two categories: three long bonds (3.02–3.28 Å) and two short bonds (2.73–2.76 Å). The Au−P bond lengths in Au_{60} are in the range of 2.24–2.32 Å, which are typical Au−P bond distances. The Au–Se bonds can also be divided into two categories: 1) the normal format, that is, (*R*)-Se-$(Au)_2$ (bond length: 2.46–2.50 Å); 2) the bare Se (highlighted in magenta, Figure 2, right) without the phenyl tail: Se-$(Au)_5$. In previous work, Fenske have reported $[Au_{10}Se_5(dppa)_4\{Co_2(CO)_5\}_4]$ and $[Au_{18}Se_8(dppthph)_6]Cl_2$, and similar Se-$(Au)_3$ motifs in the absence of the phenyl tail were also observed.[27] In these structures, the Se is three coordinated (Se-M_3, M = R or Au), and the Au–Se distances in Se-$(Au)_3$ is 2.45 ± 0.02 Å (similar to that in (*R*)-Se-$(Au)_2$). By contrast, the Se atom in our study is coordinated with five Au atoms, and the Au–Se bond length is 2.65 ± 0.02 Å (significantly longer than that of Se-M_3). The two sets of Se-$(Au)_5$ seem like two open hands, tightly connecting the five Au_{13} building blocks through the radial Au–Se bonds. This bonding mode (Se-$(Au)_5$) is the first example in the selenolate-capped gold NCs.

The formula of the nanocluster was confirmed by matrix-assisted laser desorption ionization mass spectrometry (MALDI-MS) analysis (Figure 3). MALDI-MS (positive ion

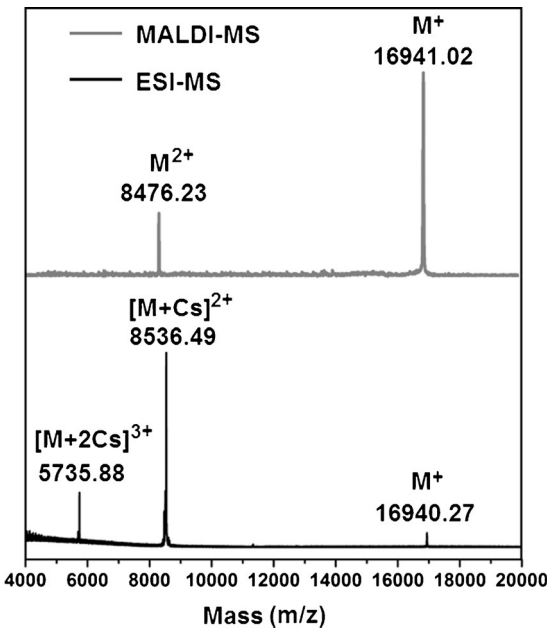

Figure 3. The mass spectrum analysis of $[Au_{60}Se_2(Ph_3P)_{10}(SePh)_{15}]^+$ NCs (positive mode).

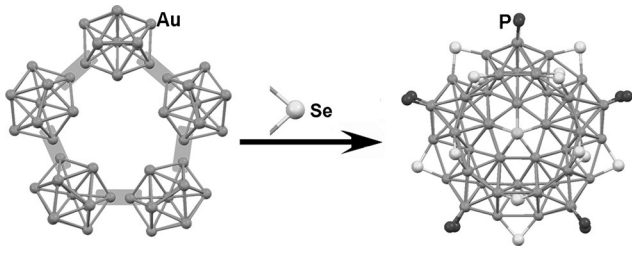

Figure 2. The core structure of $[Au_{60}Se_2(PPh_3)_{10}(SePh)_{15}]^+$. The Au atoms are gray, selenium atoms light gray, phosphorus atoms dark gray.

mode) revealed a prominent peak at $m/z = 16941.02$ Da, which is assigned to the *intact* $[Au_{60}Se_2(Ph_3P)_{10}(SePh)_{15}]^+$ nanocluster (calculated formula weight: 16941.10 Da). Furthermore, the peak at $m/z = 8470.52$ Da corresponds to the $[Au_{60}Se_2(Ph_3P)_{10}(SePh)_{15}]^{2+}$ production. The triphenylphosphine-stabilized Au NCs hardly gave rise to intact ion peaks in MALDI-MS; for example, $[Au_{11}(PPh_3)_8Cl_2]^+$, $[Au_{13}(dppe)_5Cl_2]^{3+}$ and $[Au_{25}(PPh_3)_{10}(SC_2H_4Ph)_5Cl_2]^{2+}$ NCs are all

fragmented in MALDI mass spectra analysis (see Figure S3). These observations may indicate that the Au_{60} nanocluster is electronically more stable. Furthermore, we also performed electrospray ionization mass spectrometry (ESI-MS) analysis on Au_{60} nanocluster (Figure 3), and the result is consistent with the MALDI-MS. Moreover, the purity of the product was confirmed by thermogravimetric analysis (TGA), and a 29.96 wt% loss was observed (Figure S4), consistent with the calculated loss (30.22%) according to the formula.

With respect to the optical absorption spectrum, the Au_{60} nanocluster (dissolved in CH_2Cl_2) shows five stepwise peaks at 353, 435, 510, 600, and 835 nm (Figure 4A). As Nobusada pointed out,[40] the icosahedral Au_{13} cluster is spherically symmetric, and the broken symmetry does not affect either the orbital symmetry or the energies. So, the peaks at 353 nm, 435 nm and 510 nm can be assigned to the electronic transitions within the individual Au_{13} unit. Due to the interaction among the five Au_{13} units, both the HOMO and LUMO electronic states will be changed. Therefore, the absorption peak at 835 nm is assigned to a new electronic transition because of the pentamer structure. As shown in Figure 4A, the HOMO–LUMO peak shifts from about 500 nm (Au_{13}) to 670 (Au_{25}) to 850 nm (Au_{60}), we note that Se versus S and aromatic versus nonaromatic ligands also lead to a slight redshift. As for the valence electrons, the total number of valence electrons of the Au_{60} nanocluster is 40 ($40 = 60\text{-}15\times1\text{-}2\times2\text{-}1$), corresponding to a closed shell in the jellium model. Furthermore, since the Au_{60} nanocluster is composed of five Au_{13} block buildings, the 40 valence electrons also fit the Mingos' electron counting rule ($40 = 8\times5$; the number of the Au_{13} units). Considering the theoretically predicted $[Au_{37}(PPh_3)_{10}(SR)_{10}Cl_2]^+$ by Nobusada and Iwasa,[40] we got some striking findings: 1) our results once again verified the previous proposals that the electronic properties of the building block (Au_{13} units) in the cluster-assembled materials would be retained; 2) the optical absorption properties of the cluster-assembled materials can be adjusted by controlling the number of the building block (Au_{13} units); 3) the arrangement of the building blocks will affect the electronic transitions of the whole cluster-assembled material. These findings will provide new insights in the design and synthesis of relatively large cluster-assembled materials.

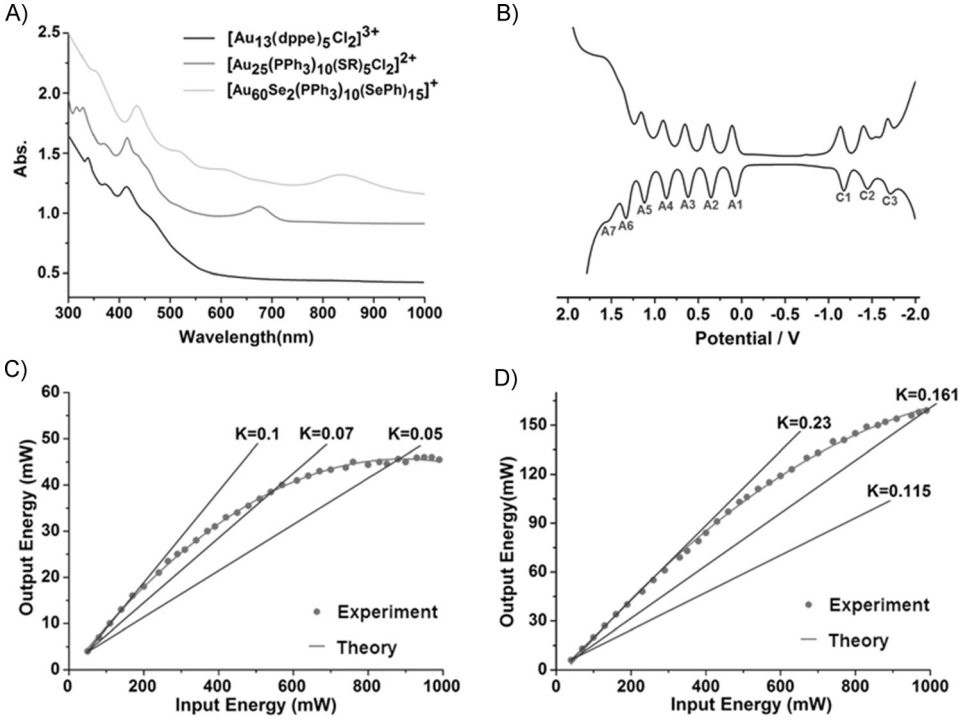

Figure 4. A) Comparison of the UV/Vis absorption spectra of $[Au_{13}(dppe)_5Cl_2]^{3+}$, $[Au_{25}(PPh_3)_{10}(SR)_5Cl_2]^{2+}$, and $[Au_{60}Se_2(PPh_3)_{10}(SePh)_{15}]^+$ NCs (in CH_2Cl_2). B) Differential pulse voltammetry of $[Au_{60}Se_2(Ph_3P)_{10}(SePh)_{15}]^+$ clusters at room temperature (in CH_2Cl_2). Optical-limiting curves of the C) Au_{60} and D) $[Au_{25}(PPh_3)_{10}(SR)_5Cl_2]^{2+}$ NCs.

To investigate the electrochemical property of the Au_{60} nanocluster, we performed differential pulse voltammetry (DPV) of the Au_{60} nanocluster at room temperature in 0.1 M Bu_4NPF_6-CH_2Cl_2 (Figure 4B). The current peaks in the DPV scans lie at the formal potentials of the cluster charge state couples and seven oxidation peaks were found at 0.075 (A1), 0.353 (A2), 0.617 (A3), 0.865 (A4), 1.118 (A5), 1.333 (A6), and 1.548 V (A7) in the positive potential region, which corresponds to oxidation to +2, +3, +4, +5, +6, +7, and +8 charge states of the Au_{60} cluster, respectively. As can be seen in Figure 4B, the peak spacings ($\triangle V$) are gradually reduced with the increase of oxidation state and the large peak spacing (A1-A2) is about 0.28 V. Moreover, three reduction peaks were also observed at −1.178 (C1), −1.450 (C2), and −1.714 (C3) in the negative-going scan. According to the DPV of Au_{60} NCs, we determined the electrochemical HOMO–LUMO energy gap of the Au_{60} to be only about 1.25 V (i.e. the difference between A1 and C1 without subtracting the charge energy, Figure 4B), which is smaller than that (about 1.62 V) of the $[Au_{25}(PPh_3)_{10}(SR)_5Cl_2]^{2+}$,[41] and is also substantially smaller than that (1.76 V) of an icosahedral Au_{13} cluster that was assigned as $Au_{13}(PPh_3)_4(SC_{12}H_{25})_2Cl_2$ by Menard and co-workers.[42]

To further explore the properties of the Au_{60} nanocluster, we performed the optical-limiting tests by measuring the power-dependent optical transmission at $\lambda = 850$ with a 1 mm cell of the Au_{60} and $[Au_{25}(PPh_3)_{10}(SR)_5Cl_2]^{2+}$ NCs (where R = $PhCH_2CH_2$) in DMSO at 3.0×10^{-3} mol L^{-1} and 20×10^{-3} mol L^{-1} (based on the Au atoms), respectively. As

shown in Figure 4C, the optical response of the Au_{60} NCs obeys Beer's law at low energy, while starts to deviate from the normal linear behavior as the input light power reaches about 140 mW. The damaging threshold and the optical limiting threshold of Au_{60} NCs in DMSO solution is determined to be 540 and 880 mW, respectively. Although the nonlinear optical property of the $[Au_{25}(PPh_3)_{10}(SR)_5Cl_2]^{2+}$ NCs was observed at the higher concentration (based on the Au atoms) and the damaging threshold was determined as 990 mW in Figure 4D, the limiting threshold does not lies in the range of 50–1000 mW. Moreover, the optical-limiting curves of the Au_{60} and $[Au_{25}(PPh_3)_{10}(SR)_5Cl_2]^{2+}$ NCs with different concentrations were also obtained (Figure S5). As can be seen in Figure S5C, the reduced concentrations results in the weaker optical-limiting effect. When the concentration of $[Au_{25}(PPh_3)_{10}(SR)_5Cl_2]^{2+}$ in DMSO increases to 60×10^{-3} mol L^{-1}, good optical-limiting effect was observed. Control experiment with $HAuCl_4$ in H_2O at high concentration (0.2 mol L^{-1}) shows no optical-limiting effect at $\lambda = 850$ nm (Figure S5A), thus the optical limiting is intrinsic to the NCs. Our results indicate the Au_{60} nanocluster exhibits a better optical-limiting effect than that of $[Au_{25}(PPh_3)_{10}(SR)_5Cl_2]^{2+}$ nanaocluster.

In summary, we have successfully synthesized $[Au_{60}Se_2(Ph_3P)_{10}(SePh)_{15}](SbF_6)$ by the reaction of phosphine-capped, polydisperse Au nanoparticles with PhSeH. The crystal structrue determined by X-ray crystallographic revealed that the framework of Au_{60} containing five icosahedral Au_{13} units clipped together by Au–Se–Au linkages sharing five vertex atoms. In this nanocluster, the small Au_{13} cluster acts as a building block, and could form the cluster-assembled materials through highly ordered arrangements. The present study provides new insights in understanding the atomic structure and arrangement of cluster-assembled materials, and some larger cluster-assembled materials with different configuration and better optical properties could be prepared by using different ligands (thiolate, selenol or others).

Experimental Section

Briefly, $HAuCl_4{\cdot}3H_2O$ (0.1576 g, 0.4 mmol) was dissolved in 5 mL nanopure water, and TOAB (0.2558 g, 0.47 mmol) was dissolved in 10 mL toluene. These two solutions were combined in a 25 mL tri-neck round-bottom flask. The solution was vigorously stirred (about 1100 rpm) with a magnetic stir bar to facilitate phase transfer of Au^{III} salt into the toluene phase. After about 15 minutes, the phase transfer was completed, leaving a clear aqueous phase at the bottom of the flask; the aqueous was then removed. The toluene solution of Au^{III} was cooled to 0°C in an ice bath over 30 minutes without stirring. Then, Ph_3P (0.315 g, 1.2 mmol) was added into the toluene solution of Au^{III}. After ≈5 min, 5 mL ice-cold aqueous solution of $NaBH_4$ (0.08 g, 2.11 mmol) was rapidly added with vigorously stirring. This led to the formation of the $Au_n(Ph_3P)_m$ clusters. After about 1 h, PhSeH (50 μL, 4.76 mmol) was directly added to the toluene solution of the $Au_n(Ph_3P)_m$ clusters without any treatment. Then, the reaction was allowed to proceed for 36 h. After that, the aqueous phase was removed. The mixture in the organic phase was rotavaporated, and then washed several times with ethanol to remove the redundant PhSeH, Ph_3P, and by-products until the optical absorption spectrum shows five stepwise peaks at 353, 435, 510, 600, and 835 nm. Finally, the pure Au_{60} NCs were obtained. The $[Au_{11}(PPh_3)_8Cl_2]^+$ NCs were synthesized by the method reported by Hutchison and co-workers.[5] the $[Au_{13}(dppe)_5Cl_2]^{3+}$ NCs were synthesized by the method reported by Shichibu and Konishi.[6c] The $[Au_{25}(PPh_3)_{10}(SC_2H_4Ph)_5Cl_2]^{2+}$ NCs were synthesized by the methods by Tsukuda and co-workers.[28]

Keywords: cluster-assembled materials · crystallography · gold nanoclusters · selenolate · surface chemistry

How to cite: *Angew. Chem. Int. Ed.* **2015**, *54*, 8430–8434
Angew. Chem. **2015**, *127*, 8550–8554

[1] a) G. Schmid, *Chem. Soc. Rev.* **2008**, *37*, 1909–1930; b) G. Schmid, *J. Cluster Sci. J. Clust. Sci.* **2014**, *25*, 29–49; c) S. Knoppe, T. Bürgi, *Acc. Chem. Res.* **2014**, *47*, 1318–1326; d) Z. Luo, A. Castleman, *Acc. Chem. Res.* **2014**, *47*, 2931–2940.
[2] M. McPartlin, R. Mason, L. Malatesta, *J. Chem. Soc. Chem. Commun.* **1969**, 334–334.
[3] M. Manassero, L. Naldini, M. Sansoni, *J. Chem. Soc. Chem. Commu.* **1979**, 385–386.
[4] C. E. Briant, B. R. C. Theobald, J. W. White, L. K. Bell, D. M. P. Mingos, A. J. Welch, *J. Chem. Soc. Chem. Commun.* **1981**, 201–202.
[5] L. McKenzie, T. Zaikova, J. Hutchison, *J. Am. Chem. Soc.* **2014**, *136*, 13426–13435.
[6] a) Y. Shichibu, Y. Kamei, K. Konishi, *Chem. Commun.* **2012**, *48*, 7559–7561; b) Y. Shichibu, K. Suzuki, K. Konishi, *Nanoscale* **2012**, *4*, 4125–4129; c) Y. Shichibu, K. Konishi, *Small* **2010**, *6*, 1216–1220; d) Y. Shichibu, M. Zhang, Y. Kamei, K. Konishi, *J. Am. Chem. Soc.* **2014**, *136*, 12892–12895.
[7] B. K. Teo, X. Shi, H. Zhang, *J. Am. Chem. Soc.* **1992**, *114*, 2743–2745.
[8] X. Wan, Z. Lin, Q. Wang, *J. Am. Chem. Soc.* **2012**, *134*, 14750–14752.
[9] B. S. Gutrath, I. M. Oppel, O. Presly, I. Beljakov, V. Meded, W. Wenzel, U. Simon, *Angew. Chem. Int. Ed.* **2013**, *52*, 3529–3532; *Angew. Chem.* **2013**, *125*, 3614–3617.
[10] G. Schmid, R. Pfeil, R. Boese, F. Bandermann, S. Meyer, G. H. M. Calis, J. W. A. vander Velden, *Chem. Ber.* **1981**, *114*, 3634–3642.
[11] Y. Yanagimoto, Y. Negishi, H. Fujihara, T. Tsukuda, *J. Phys. Chem. B* **2006**, *110*, 11611–11614.
[12] J. Chen, Q. Zhang, T. A. Bonaccorso, P. G. Williard, L. Wang, *J. Am. Chem. Soc.* **2014**, *136*, 92–95.
[13] a) H. Qian, M. Zhu, Z. Wu, R. Jin, *Acc. Chem. Res.* **2012**, *45*, 1470–1479; b) H. Qian, D. Jiang, G. Li, C. Gayathri, A. Das, R. R. Gil, R. Jin, *J. Am. Chem. Soc.* **2012**, *134*, 16159–16162; c) H. Qian, W. T. Eckenhoff, Y. Zhu, T. Pintauer, R. Jin, *J. Am. Chem. Soc.* **2010**, *132*, 8280–8281.
[14] J. Nishigaki, R. Tsunoyama, H. Tsunoyama, N. Ichikuni, S. Yamazoe, Y. Negishi, M. Ito, T. Matsuo, K. Tamao, T. Tsukuda, *J. Am. Chem. Soc.* **2012**, *134*, 14295–14297.
[15] E. S. Shibu, T. Pradeep, *Chem. Mater.* **2011**, *23*, 989–999.
[16] A. Dass, *J. Am. Chem. Soc.* **2011**, *133*, 19259–19261.
[17] P. J. Krommenhoek, J. Wang, N. Hentz, A. C. Johnston-Peck, K. A. Kozek, G. Kalyuzhny, J. B. Tracy, *ACS Nano* **2012**, *6*, 4903–4911.
[18] Z. Tang, D. A. Robinson, N. Bokossa, B. Xu, S. Wang, G. Wang, *J. Am. Chem. Soc.* **2011**, *133*, 16037–16044.
[19] P. D. Jadzinsky, G. Calero, C. J. Ackerson, D. A. Bushnell, R. D. Kornberg, *Science* **2007**, *318*, 430–433.
[20] M. W. Heaven, A. Dass, P. S. White, K. M. Holt, R. W. Murray, *J. Am. Chem. Soc.* **2008**, *130*, 3754–3755.
[21] M. Zhu, C. M. Aikens, F. J. Hollander, G. C. Schatz, R. Jin, *J. Am. Chem. Soc.* **2008**, *130*, 5883–5885.
[22] a) C. Zeng, T. Li, A. Das, N. L. Rosi, R. Jin, *J. Am. Chem. Soc.* **2013**, *135*, 10011–10013; b) C. Zeng, H. Qian, T. Li, G. Li, N. L. Rosi, B. Yoon, R. N. Barnett, R. L. Whetten, U. Landman, R.

Jin, *Angew. Chem. Int. Ed.* **2012**, *51*, 13114 – 13118; *Angew. Chem.* **2012**, *124*, 13291 – 13295.
[23] a) Y. Negishi, W. Kurashige, U. Kamimura, *Langmuir* **2011**, *27*, 12289 – 12292; b) W. Kurashige, M. Yamaguchi, K. Nobusada, Y. Negishi, *J. Phys. Chem. Lett.* **2012**, *3*, 2649 – 2652; c) W. Kurashige, S. Yamazoe, K. Kanehira, T. Tsukuda, Y. Negishi, *J. Phys. Chem. Lett.* **2013**, *4*, 3181 – 3185.
[24] X. Meng, Q. Xu, S. Wang, M. Zhu, *Nanoscale* **2012**, *4*, 4161 – 4165.
[25] Q. Xu, S. Wang, Z. Liu, G. Xu, X. Meng, M. Zhu, *Nanoscale* **2013**, *5*, 1176 – 1182.
[26] a) Y. Song, T. Cao, H. Deng, X. Zhu, P. Li, M. Zhu, *Sci. China Chem.* **2014**, *57*, 1218 – 1224; b) Y. Song, J. Zhong, S. Yang, S. Wang, T. Cao, J. Zhang, P. Li, D. Hu, Y. Pei, M. Zhu, *Nanoscale* **2014**, *6*, 13977 – 13985; c) Y. Song, S. Wang, J. Zhang, X. Kang, S. Chen, P. Li, H. Sheng, M. Zhu, *J. Am. Chem. Soc.* **2014**, *136*, 2963 – 2965.
[27] a) P. Sevillano, O. Fuhr, O. Hampe, S. Lebedkin, C. Neiss, R. Ahlrichs, D. Fenske, M. Kappes, *Eur. J. Inorg. Chem.* **2007**, 5163 – 5167; b) P. Sevillano, O. Fuhr, D. Fenske, *Z. Anorg. Allg. Chem.* **2007**, *633*, 1783 – 1786.
[28] Y. Shichibu, Y. Negishi, T. Watanabe, N. K. Chaki, H. Kawaguchi, T. Tsukuda, *J. Phys. Chem. C* **2007**, *111*, 7845 – 7847.
[29] a) H. Qian, M. Zhu, E. Lanni, Y. Zhu, M. E. Bier, R. Jin, *J. Phys. Chem. C* **2009**, *113*, 17599 – 17603; b) H. Qian, W. T. Eckenhoff, M. E. Bier, T. Pintauer, R. Jin, *Inorg. Chem.* **2011**, *50*, 10735 – 10739.
[30] A. Das, T. Li, K. Nobusada, Q. Zeng, N. L. Rosi, R. Jin, *J. Am. Chem. Soc.* **2012**, *134*, 20286 – 20289.
[31] N. Rosi, D. Giljohann, C. Thaxton, A. Lytton-Jean, M. Han, C. Mirkin, *Science* **2006**, *312*, 1027 – 1030.
[32] H. Wohltjen, A. W. Snow, *Anal. Chem.* **1998**, *70*, 2856 – 2859.
[33] C. Huang, C. Chiang, Z. Lin, K. Lee, H. Chang, *Anal. Chem.* **2008**, *80*, 1497 – 1504.
[34] C. Lin, T. Yang, C. Lee, S. Huang, R. Sperling, M. Zanella, J. Li, J. Shen, H. Wang, H. Yeh, W. Parak, W. Chang, *ACS Nano* **2009**, *3*, 395 – 401.
[35] M. Zhu, C. M. Aikens, M. P. Hendrich, R. Gupta, H. Qian, G. C. Schatz, R. Jin, *J. Am. Chem. Soc.* **2009**, *131*, 2490 – 2492.
[36] S. Antonello, N. Perera, M. Ruzzi, J. Gascón, F. Maran, *J. Am. Chem. Soc.* **2013**, *135*, 15585 – 15594.
[37] H. Chong, P. Li, S. Wang, F. Fu, J. Xiang, M. Zhu, Y. Li, *Sci. Rep.* **2013**, *3*, 3214 – 3217.
[38] G. Li, R. Jin, *Acc. Chem. Res.* **2013**, *46*, 1749 – 1758.
[39] B. K. Teo, H. Zhang, X. Shi, *J. Am. Chem. Soc.* **1990**, *112*, 8552 – 8562.
[40] K. Nobusada, T. Iwasa, *J. Phys. Chem. C* **2007**, *111*, 14279 – 14282.
[41] S. Park, D. Lee, *Langmuir* **2012**, *28*, 7049 – 7054.
[42] L. D. Menard, S. P. Gao, H. Xu, R. D. Twesten, A. S. Harper, Y. Song, G. Wang, A. D. Douglas, J. C. Yang, A. I. Frenkel, R. G. Nuzzo, R. W. Murray, *J. Phys. Chem. B* **2006**, *110*, 12874 – 12883.
[43] CCDC 1060824, contain the supplementary crystallographic data for this paper. These data can be obtained free of charge from The Cambridge Crystallographic Data Centre via www.ccdc.cam.ac.uk/data_request/cif.

Received: February 25, 2015
Revised: April 14, 2015
Published online: May 27, 2015

